Quasielastic transfer reactions induced by ^{56}Fe on ^{58}Ni, ^{64}Ni, and ^{122}Sn

S. Pontoppidan, P. R. Christensen, Ole Hansen,* and F. Videbaek
Niels Bohr Institute, University of Copenhagen, DK-2100 Copenhagen, Denmark

H. C. Britt, B. H. Erkkila, Y. Patin,† R. H. Stokes, and M. P. Webb
Los Alamos National Laboratory, Los Alamos, New Mexico 87545

R. L. Ferguson, F. Plasil, and G. R. Young
Oak Ridge National Laboratory, Oak Ridge, Tennessee 37830
(Received 14 March 1983)

Differential cross sections $\sigma(Z,A,E,\theta)$ for the quasielastic projectilelike reaction products from the bombardment of ^{56}Fe on ^{58,64}Ni and ^{122}Sn at 5.9 and 8.5 MeV/nucleon have been measured with a channel-plate time-of-flight telescope followed by a ΔE-E gas-ionization chamber. Angular intervals of 10°—15° centered at the grazing angles were covered. The differential cross sections for one-proton transfer with Q values near zero were analyzed using the distorted-wave Born approximation, which can account for the shape of the angular distributions and, to better than a factor of 5, for the absolute cross sections. At Q values more negative than -10 MeV the measured angular distributions begin to deviate from the distorted-wave Born approximation predictions. Substructures were observed in the energy spectra near $Q=-25$ MeV. A model for unfolding the effects of particle evaporation from the reaction products is developed. It is shown that, within the limitations of the model, the observed substructures cannot be accounted for by evaporation effects alone but must be present in the primary energy spectra. Finally the optimum Q values are analyzed with a one-body dissipation model. The model is reasonably successful if the concept of a local Fermi momentum is introduced.

[NUCLEAR REACTIONS Heavy ions ^{58,64}Ni, ^{122}Sn(^{56}Fe,X), $E=320$, 460 MeV; measured $\sigma(Z,A,Q,\theta)$. Substructures in energy spectra, DWBA analysis, evaporation analysis, Q_{opt} values, transfer-induced energy loss.]

I. INTRODUCTION

Quasielastic reactions induced by beams heavier than chlorine have been relatively unexplored due to the experimental difficulties encountered in obtaining the charge and mass resolution necessary to observe individual isotopes. Data on elastic and inelastic scattering with adequate energy, charge, and mass resolution have been reported for only two systems, ^{40}Ar + ^{208}Pb (Ref. 1) and ^{86}Kr + ^{208}Pb.[2]

For energy losses larger than 25 MeV, experiments done with identical nuclei in the entrance channel, ^{40}Ca + ^{40}Ca,[3] ^{56}Fe + ^{56}Fe,[4] and ^{63}Cu + ^{63}Cu,[3] have revealed narrow structures in the energy spectra for individual isotopes. Excitation of high multipolarity giant resonances[3] or light-particle evaporation from primary reaction fragments[5] had been suggested as the origin of these structures, but at present no generally accepted explanation has been given.

The goals of the present experiments were threefold: (1) to investigate the systematics of cross section angular distribution at Q values close to 0 MeV and, in particular, to test whether DWBA can account for the observations; (2) to search for structures in the energy spectra; and (3) to investigate the systematics of the Q value of the maximum quasielastic cross section (Q_{opt}) as a function of the bombarding energy, mass transfer, and target.

Section II of the paper details the experimental techniques, while the data are presented in Sec. III. Section IV contains the discussion. In Sec. IV A a DWBA analysis of the one-proton stripping cross sections is presented, while Sec. IV B is a discussion of the shapes of the observed energy spectra in terms of a model for unfolding the particle evaporation contribution from the measured spectra. An account of the observed Q_{opt} values in terms of a one-body dissipation model is presented in Sec. IV C. Finally Sec. V contains a summary.

Parts of the data, concerning first and second moments of the observed Z and N distributions of the reaction products, have been published separately.[6]

II. EXPERIMENTAL PROCEDURE AND DATA REDUCTION

A. Procedure

Beams of ^{56}Fe having energies of 5.9 or 8.5 MeV/nucleon were obtained from the Lawrence Berkeley Laboratory SuperHILAC. The beam was collimated by two 3×3-mm^2 slits located 187 cm and 61 cm, respectively, from the target. The Ni targets were self-supporting metal foils with thicknesses of 0.6 mg/cm^2 (^{58}Ni) and 0.9 mg/cm^2 (^{64}Ni). Each isotope was enriched to greater than

TABLE I. List of experiments.

Target	E_{lab} (MeV)	θ_{lab} (deg)						
^{58}Ni	460	6	9	12	14	16		
^{58}Ni	315	14	17	20	23			
^{64}Ni	460	6	9	12	14	16		
^{122}Sn	460	12	16	18	20	22	24	26
^{122}Sn	320	27	31	35	38.5	42		

98%. The ^{122}Sn targets had a 5-μg/cm^2 carbon backing, thicknesses of approximately 1 mg/cm^2, and isotopic purity of 97%. A list of the experiments is given in Table I.

The charged particles emerging from the target drifted through a 163-cm-long time-of-flight (TOF) path and entered a ΔE-E telescope. The TOF system consisted of two identical channel plate detectors[7] and had an intrinsic time resolution of 80 ps for elastically scattered ^{56}Fe. The ΔE-E counter, consisting of a gas-ionization chamber and a Si surface-barrier detector, is identical to the one described in Ref. 8. The detection system subtended a solid angle of 0.023 msr. A solid-state detector was used as a monitor.

For each event four signals were recorded: ΔE, E, the TOF ΔT, and a timing signal derived from the surface-barrier detector and the anode of the ionization chamber. This last signal depended linearly on the vertical position of the detected particle in the ionization chamber.

B. Data reduction

The off-line data analysis was performed on the RC4000 computer system at the Niels Bohr Institute. For each event $E_{tot}=\Delta E+E_{stop}$ was used to derive the kinetic energy of the detected nucleus between the TOF foils (E_f) and in the middle of the target (E_{reac}). In the correction for energy loss in the foils, the mass chosen for each Z was that of the most stable isotope, except for the elements $Z=24$–28, where for each Z the mass of the most abundant isotope was used. In addition, the reaction Q value was calculated by assuming binary kinematics. The ΔE and ΔT signals were software corrected for pulse-height drifts by stabilizing on the elastic peak. The ΔT signal was further corrected for its dependence on the vertical position signal.

The Z determination was made at each angle by identifying the ridge belonging to a given value of Z in a plot of $(\Delta E+0.08E_{tot})$ vs E_{tot}, starting from the conspicuous Fe line. This procedure was performed by an algorithm based on the principles given in Ref. 9. The position of each Z ridge was fitted by a polynomial in E_{tot}; Fig. 1 shows an example of the resulting Z vs E_{tot} plot.

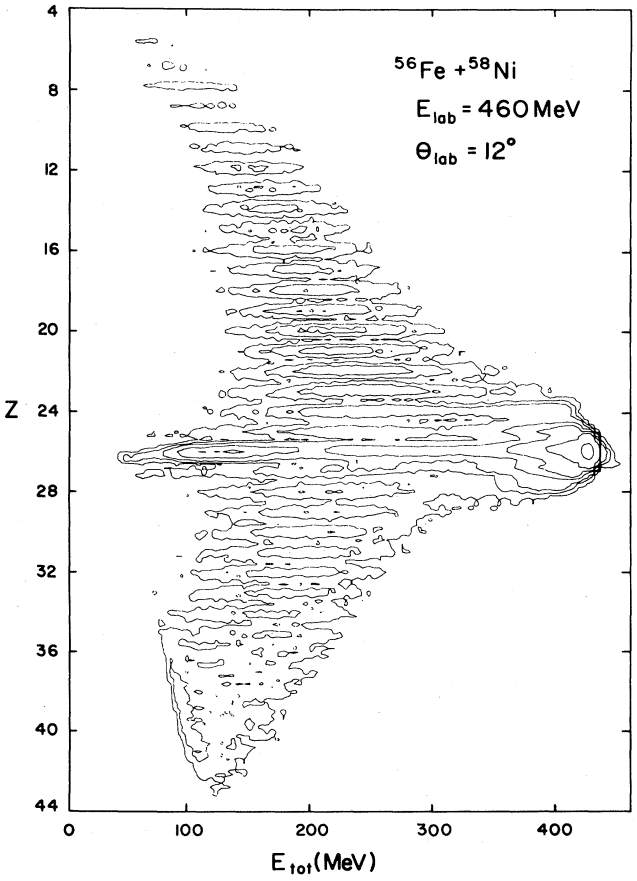

FIG. 1. Contour plot of Z vs E_{tot}. The lines are drawn for the contour levels at 5, 20, 100, 400, 2000, and 10 000 counts per channel.

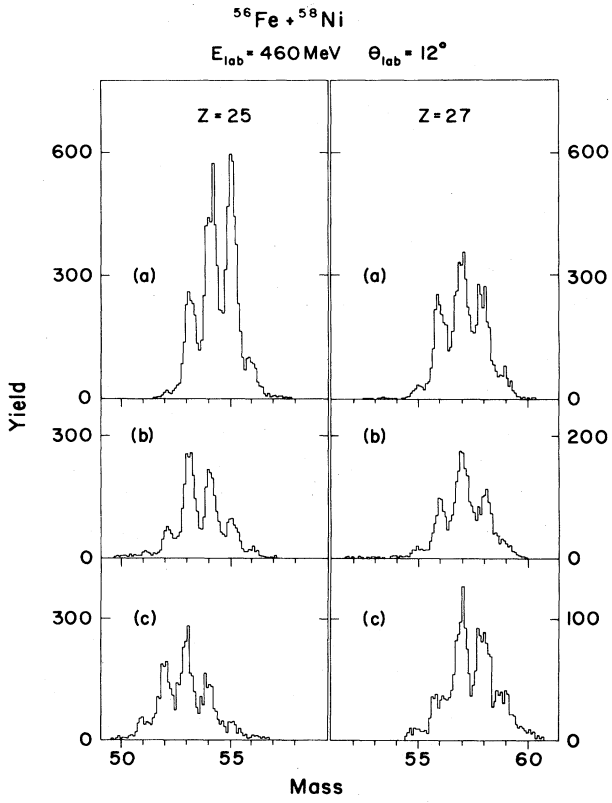

FIG. 2. Mass spectra for the elements Mn ($Z=25$) and Co ($Z=27$) at the Q-value intervals: (a) $-15>Q>-25$ MeV, (b) $-35>Q>-45$ MeV, and (c) $-150>Q>-170$ MeV.

In a process analogous to the Z definition, the mass M of the detected particle was defined from identifying the mass ridges in a plot of $E_f T^2$ vs $E_{\rm tot}$. This information was used to create a final set of data, which for each event contained the parameters Q, M, Z, $E_{\rm tot}$, $E_{\rm reac}$, ΔT, E_f, and ΔE.

The overall energy resolution of 1.2% (4—6 MeV) was primarily limited by the beam energy spread and the resolution of the ΔE-E counter. The Z resolution of $Z/\Delta Z = 50$ was determined by the energy straggling in the ionization chamber. The mass resolution of $M/\Delta M = 85$ was limited by the energy resolution of the ΔE-E counter. Figure 2 shows typical examples of mass spectra.

Relative cross sections were obtained by normalizing to the yield in the monitor counter. The absolute cross section scale was obtained by assuming that at the smallest angles the "elastic" scattering was Rutherford scattering. The uncertainties in the absolute normalizations are ±20%, except for ^{56}Fe + ^{122}Sn at 460 MeV, where the uncertainty might be as high as ±35%.

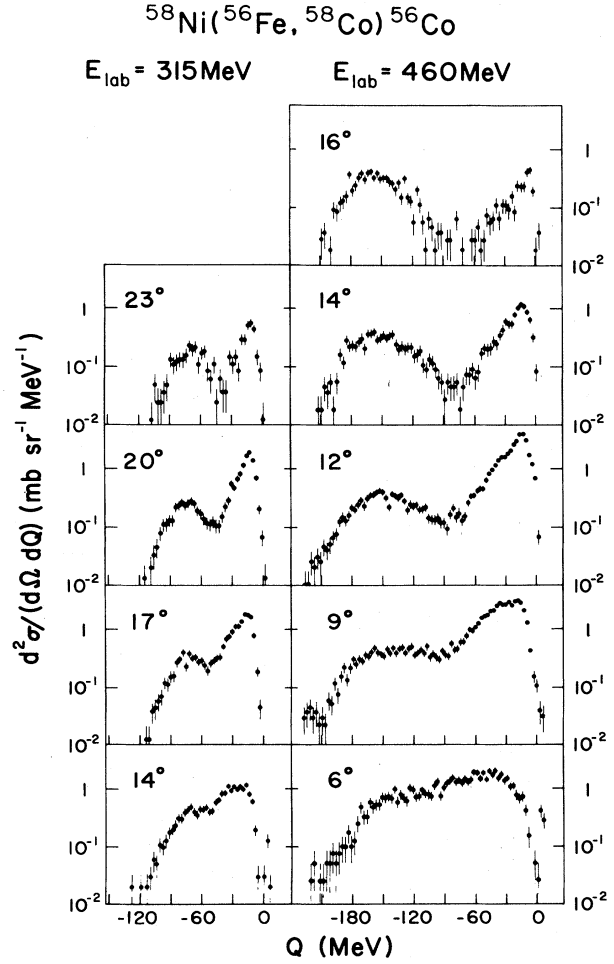

FIG. 3. Q-value spectra obtained at two different bombarding energies. Angles and cross sections refer to the laboratory system, and each point corresponds to a Q-bin size of 3 MeV. The grazing angles are 20° and 12° at $E_{\rm lab} = 315$ and 460 MeV, respectively.

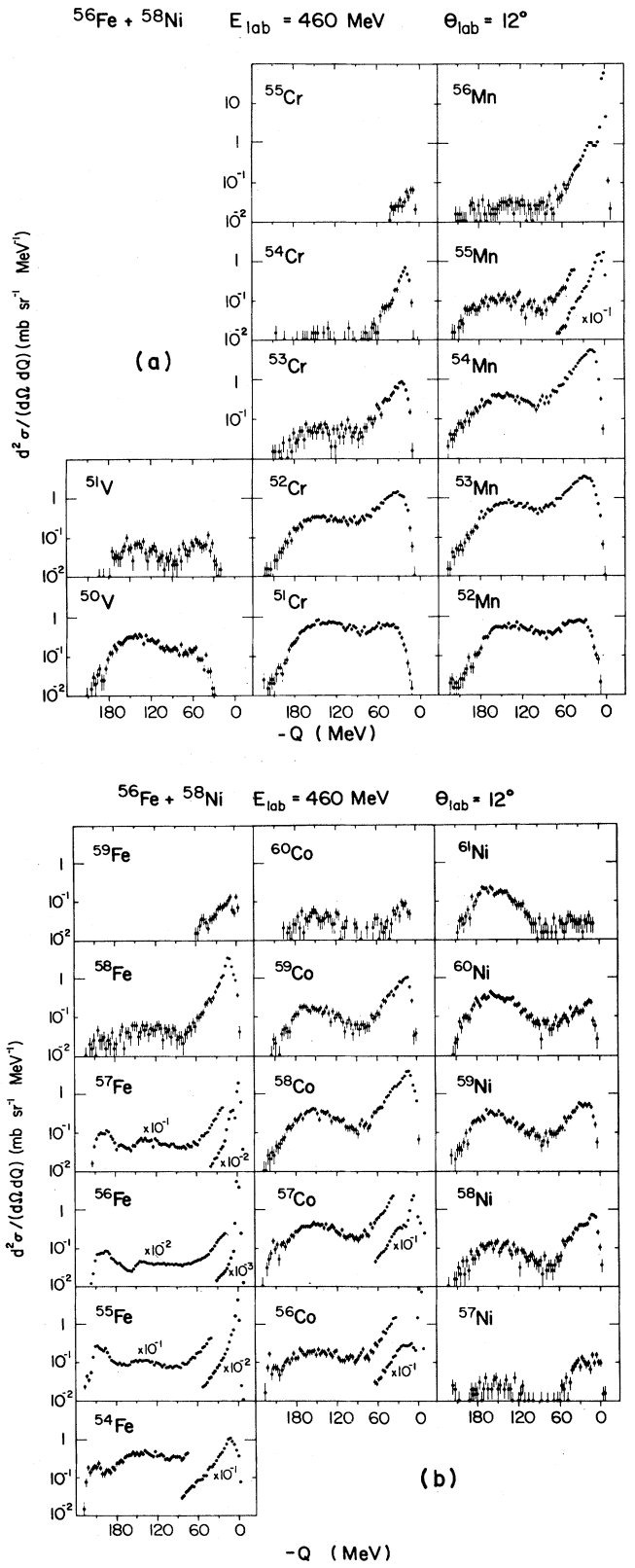

FIG. 4. Grazing angle Q-value spectra for (a) $Z = 23$, 24, and 25, and (b) $Z = 26$, 27, and 28. The cross sections are calculated in the laboratory system, and each point corresponds to a Q-bin size of 3 MeV.

III. EXPERIMENTAL RESULTS

A. Energy spectra

In Fig. 3 energy spectra from reactions on ^{58}Ni are shown. The laboratory system cross sections $d^2\sigma/d\Omega\, dQ$ of ^{58}Co ions are shown versus the binary Q value for all angles of observation and for bombarding energies 315 and 460 MeV. At both bombarding energies two distinct structures are apparent in the data for angles at or behind grazing, $\theta_{graz}=20°$ and 12°, respectively. The broad peak just below $Q=0$ MeV is referred to as the quasielastic (QE) peak, and the peak at large energy loss corresponds to deep-inelastic collisions (DIC).

No conspicuous substructures are discernible in either the QE or the DIC peaks. A possible, but weak, substructure (shoulder) may been seen at $\theta=12°$ and 14° around $Q=-25$ MeV for $E_{lab}=460$ MeV.

The V, Cr, Mn, Fe, Co, and Ni spectra for ^{56}Fe + ^{58}Ni at 460 MeV and $\theta_{lab}=12°$ are shown in Fig. 4. For $|\Delta A| \geq 2$ the spectra show the same characteristics as pointed out above, and it is further seen that the prominence of the QE group diminishes as $|\Delta A|$ increases. For $|\Delta A| \leq 1$ feed through from the elastic peak becomes a problem, rendering the $Q=0$ part of the ^{55}Fe, ^{55,56}Mn, and ^{56}Co spectra useless. The ^{56}Fe spectrum is completely dominated by slit-scattered events, and feed through from this spectrum obscures the ^{55,57}Fe spectra even in the DIC region. The overall systematics of the energy spectra for the other reactions are quite similar, and the trends observed here have been well documented in the literature.[10]

Figure 5 shows the QE part of the ^{57}Co spectra from targets of ^{58}Ni (left-hand side) and ^{64}Ni (right-hand side) at 460 MeV bombarding energy and all angles of observation. Shoulders at $Q \approx -25$ MeV are observed in the spectra for both ^{58}Ni and ^{64}Ni targets at angles ranging from 12° to 16°. QE grazing angle spectra for $|\Delta A| \leq 2$ are shown in Fig. 6. The ^{57}Co substructure is detectable for the ^{58}Ni target at both bombarding energies and for the ^{64}Ni and ^{122}Sn targets at the high bombarding energy. Other shoulders and substructures also appear in a number of other spectra, but their statistical significance is open to question. Thus the substructure phenomena previously reported in collisions between symmetric systems[3,4] seem to be of a more general character, although the shoulders observed in this work are not as numerous and pronounced as the "bumps" of Refs. 3 and 4.

B. Angular distributions and integrated cross sections

A set of typical angular distributions from the reaction ^{56}Fe + ^{58}Ni at 460 MeV, corresponding to different reaction products and different Q bins, is displayed in Fig. 7. For Q values $\gtrsim -60$ MeV they are of an approximately Gaussian shape (bell shaped). With increasing energy loss the angle for maximum cross section θ_0 moves forward and the width increases. For a specific energy loss, θ_0 is independent of ejectile (A,Z), except for $Q \gtrsim -20$ MeV where small variations are found.

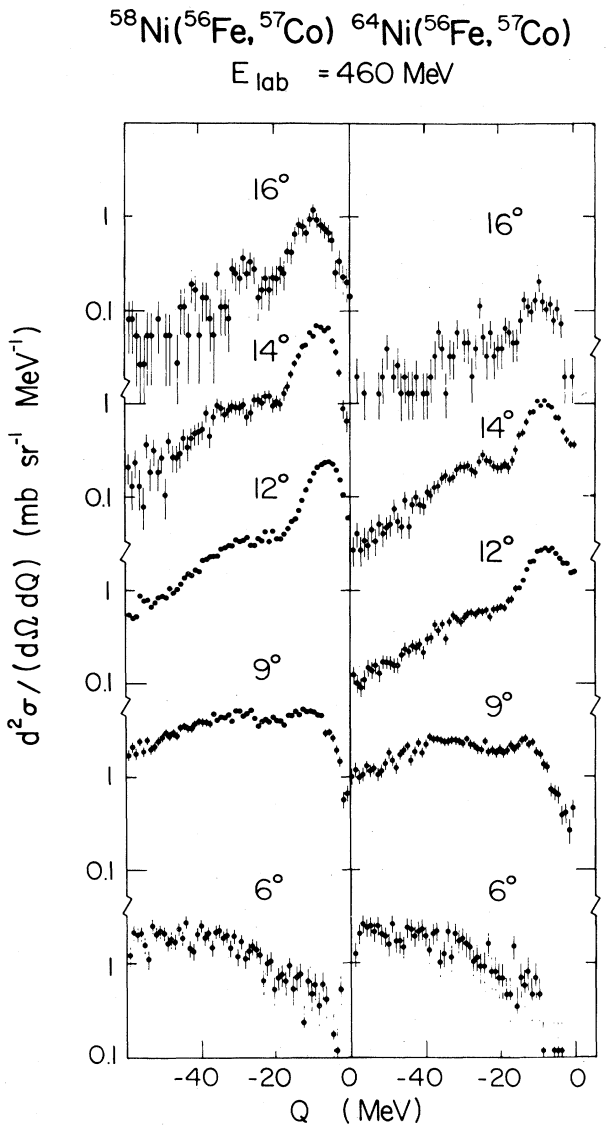

FIG. 5. Q-value spectra for the quasielastic region of ^{57}Co at five different angles obtained in the reactions ^{56}Fe (460 MeV) + ^{58,64}Ni. Angles and cross sections refer to the laboratory system, and each point corresponds to a Q-bin size of 1 MeV.

The angle integrated cross sections in the interval $0>Q>-20$ MeV are shown in Table II. The transfer cross section summed over all channels increases with bombarding energy. This is primarily due to a strong increase in the one-nucleon transfer channels, whereas most other transfer channels show a constant or even decreasing cross section. For example, the cross section is decreasing in almost all channels where three or more nucleons have been transferred. At any bombarding energy the cross section decreases sharply with an increasing number of transferred nucleons, a characteristic that becomes stronger for the heaviest targets and the highest bombarding energies. It may be pointed out that the double charge-exchange channel ^{56}Cr has a cross section of 150 μb in ^{56}Fe + ^{122}Sn at 315 MeV.

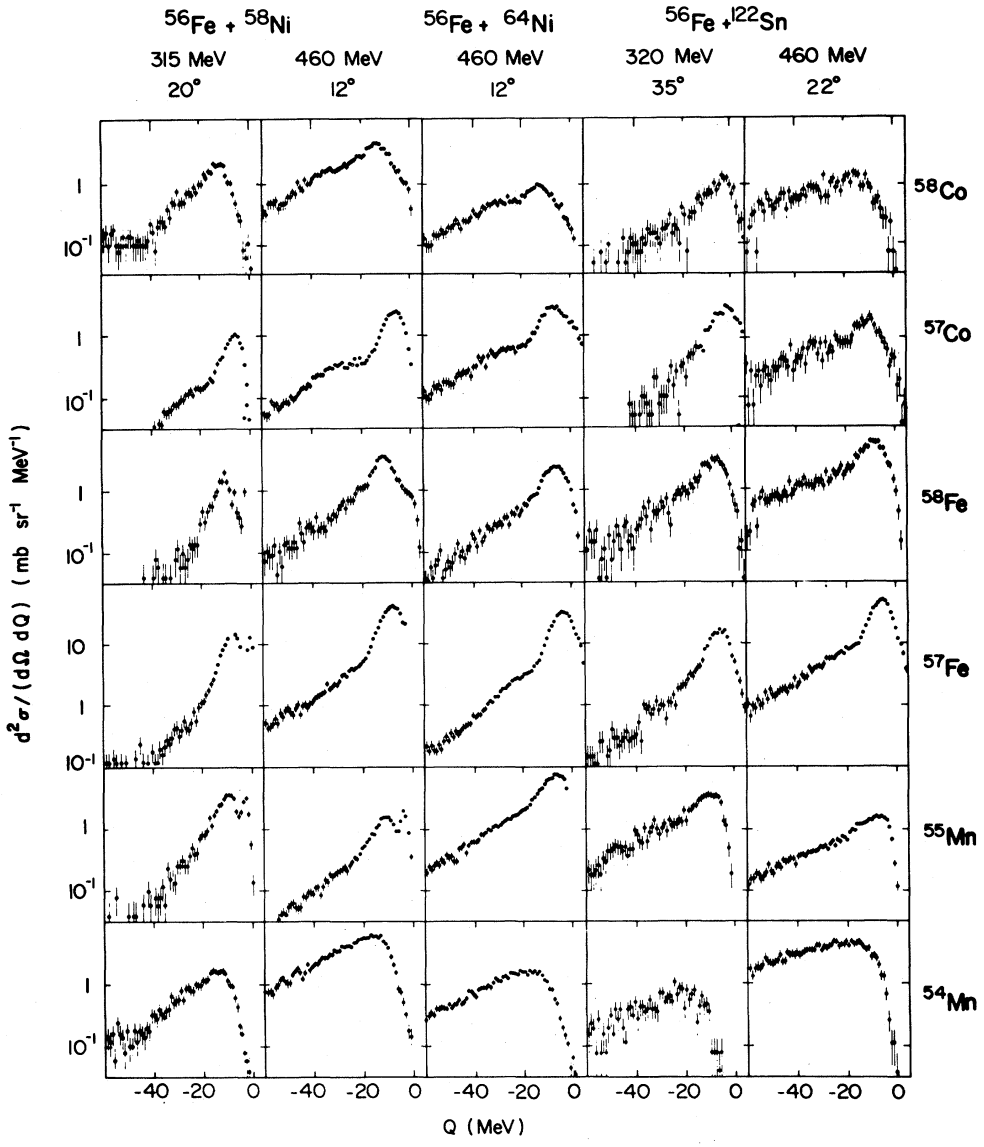

FIG. 6. Q-value spectra for the quasielastic region of six different projectilelike fragments (rows) obtained at the grazing angles of five different reactions (columns). Angles and cross sections refer to the laboratory system, and each point corresponds to a Q-bin size of 1 MeV.

C. Systematics of optimum Q values at the grazing angle

The Q value corresponding to the maximum cross section in the QE region is denoted by Q_{opt}. As long as $|\Delta M| \leq 3$ and $0 > Q > -20$ MeV, the QE peak is in most cases conspicuous enough for a determination of Q_{opt} when grazing angle spectra are considered. An effective optimum Q value, $Q_{\text{opt}}^{\text{eff}}$, which is the Q_{opt} value corrected for the contribution from the differences in the potential barriers in the entrance (i) and exit (f) channels, is defined by

$$Q_{\text{opt}}^{\text{eff}} = Q_{\text{opt}} - (V_B^f - V_B^i) = Q_{\text{opt}} - \Delta V_B \ , \tag{1}$$

where[11]

$$V_B = 1.44 Z_1 Z_2 / R_B (1 - 0.63/R_B) \ , \tag{2}$$

with

$$R_B = 1.07(A_1^{1/3} + A_2^{1/3}) + 2.72 \text{ fm} \ , \tag{3}$$

and the Z and A taken for either the entrance channel or the exit channel. The $Q_{\text{opt}}^{\text{eff}}$ values obtained from the QE data are given in Table III. $Q_{\text{opt}}^{\text{eff}}$ for a given isotope, in general, decreases with increasing bombarding energy. The $Q_{\text{opt}}^{\text{eff}}$ values for isotopes that cannot be produced in pure pickup or stripping processes are very similar to the values obtained for isotopes that can be produced this way, as long as the same total number of nucleons is

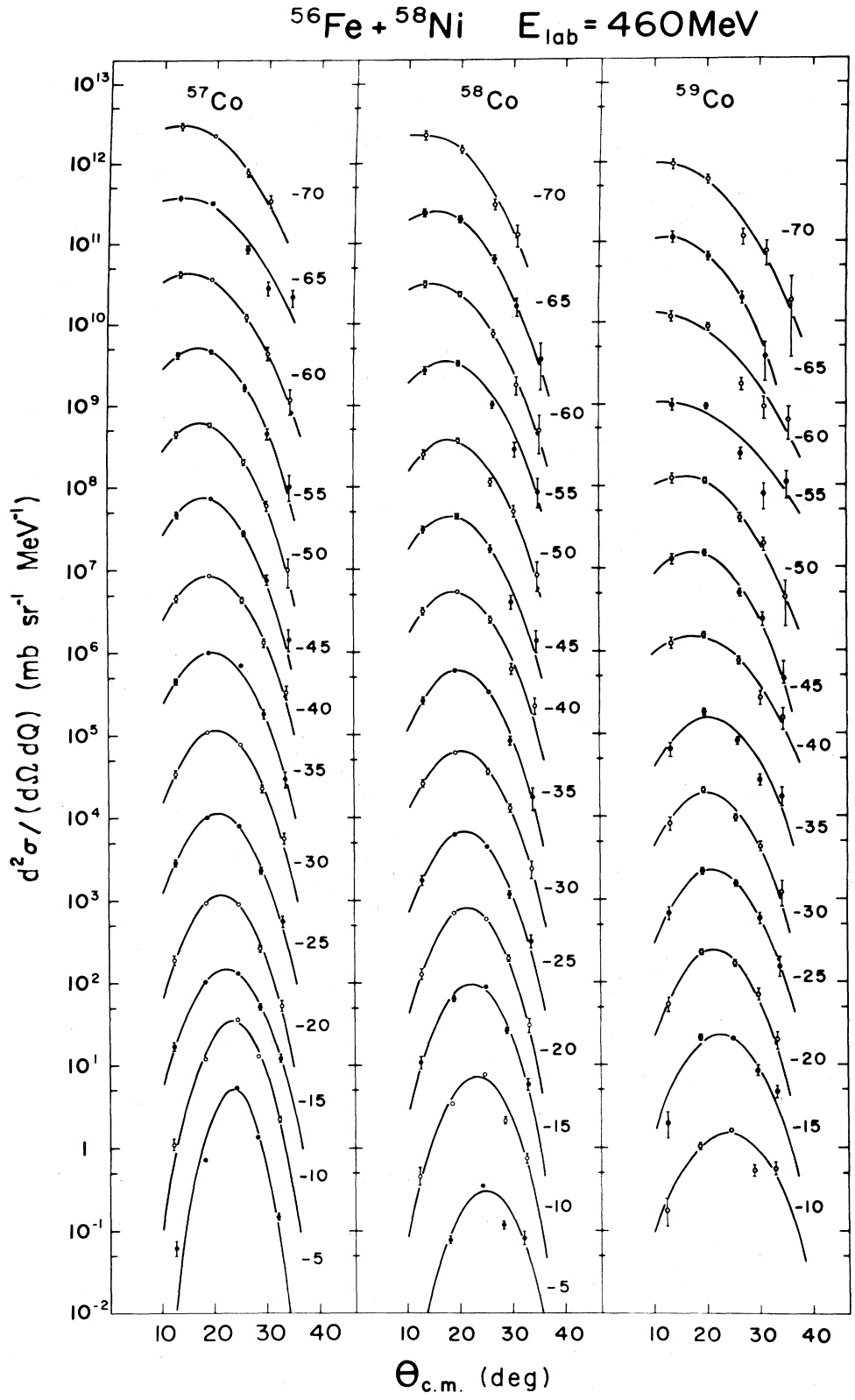

FIG. 7. Angular distributions in the center-of-mass system for ^{57,58,59}Co produced in the reaction ^{56}Fe + ^{58}Ni at E_{lab}=460 MeV. The solid lines are Gaussian fits to the data points. Each angular distribution corresponds to a Q-value bin of 5 MeV starting from $Q = -5$ MeV and ending at $Q = -70$ MeV. The c.m.s. cross section of each bin has been multiplied by $10^{(-Q/5)}$.

TABLE II. Angle-integrated cross sections for $0 > Q > -20$ MeV. All cross sections are in mb.

	A	$Z=24$	25	26	27	28	24	25	26	27	28	A	
^{58}Ni	60					1.0					0.36	60	^{58}Ni
315 MeV	59				1.4	1.4				1.4	1.4	59	460 MeV
	58			3.0	5.1	2.0			5.0	5.5	1.2	58	
	57			24	17	0.3			45	22	0.3	57	
	56		0.3		4.5			1.8		5.0		56	
	55		7.5					18				55	
	54	0.2	4.0				0.42	4.2				54	
	53	0.9	3.0				0.33	2.3				53	
	52	0.6	0.33				0.45	0.15				52	
	60									0.06	0.12	60	^{64}Ni
	59								0.27	0.84	0.15	59	460 MeV
	58								6.0	2.4	0.12	58	
	57							0.42	45	4.2	0.03	57	
	56							2.4		1.5		56	
	55						0.21	15				55	
	54						1.5	3.9				54	
	53						0.75	0.69				53	
	52						0.27					52	
^{122}Sn	60				0.33	0.06				0.15	0.03	60	^{122}Sn
320 MeV	59			2.0	1.7	0.10			1.4	1.1		59	460 MeV
	58			21					22	2.9	0.06	58	
	57		1.9	84					150	4.8		57	
	56	0.15	6.0					30				56	
	55	0.72	23				0.93	60				55	
	54	3.9	3.6				12	11				54	
	53	1.2	0.72				1.6	1.3				53	
	52	0.39					0.38					52	

TABLE III. $-Q_{\text{opt}}^{\text{eff}}$ values obtained at the grazing angle. All Q values are in MeV. Experimental uncertainties are ±1 MeV.

	A	$Z=24$	25	26	27	28	24	25	26	27	28	A	
^{58}Ni	60					12					15	60	^{58}Ni
315 MeV	59				15	15				15	18	59	460 MeV
	58			10	12	12			12	13	11	58	
	57			7	5	18			8	6		57	
	56				12							56	
	55		9					11				55	
	54	15	14				18	18				54	
	53	20	18									53	
	52	20										52	
	60										14	60	^{64}Ni
	59									17	20	59	460 MeV
	58								9	14	16	58	
	57							18	6	9		57	
	56							15		20		56	
	55						19	8				55	
	54						16					54	
^{122}Sn	59				14							59	^{122}Sn
320 MeV	58			6					9			58	460 MeV
	57		15	4					4			57	
	56		14					15				56	
	55		6					6				55	
	54	12	12									54	
	53	15	15									53	

TABLE IV. Calculated peak cross section in mb/sr.

State	λ	σ_{max} 315 MeV	σ_{max} 460 MeV
	^{58}Ni(^{56}Fe,^{55}Mn)		
$2p_{3/2}$	4, 3, 2	0.060	0.199
$2p_{1/2}$	4, 3	0.060	0.160
$1f_{5/2}$	6, 5, 4	0.271	0.621
$1g_{9/2}$	7, 6, 5	0.270	0.692
Total[a]		3.96	10.03
R[b]		0.52	0.34
	^{122}Sn(^{56}Fe,^{55}Mn)		
State	λ	σ_{max} 320 MeV	σ_{max} 464 MeV
$2d_{5/2}$	5, 4, 3	0.104	0.234
$2d_{3/2}$	5, 4, 3	0.146	0.265
$1g_{7/2}$	7, 6, 5, 4	0.191	0.341
$1h_{11/2}$	8, 7, 6	0.132	0.338
$3s_{1/2}$	3	0.029	0.035
Total[a]		3.61	7.28
R[b]		0.21	0.07

[a]Total is the sum of individual transitions times the spectroscopic factor.
[b]Ratio of $\sigma_{calc}/\sigma_{exp}(-4.5 > Q > -13.5)$.

transferred. At angles greater than the grazing angle, Q_{opt}^{eff} is nearly independent of angle; whereas for smaller angles Q_{opt}^{eff} decreases with decreasing angle.

Q_{opt}^{eff} decreases roughly linearly with the number of transferred nucleons (see Fig. 12), which indicates that on the average a constant energy is dissipated per transferred nucleon.

IV. DISCUSSION

A. Angular distributions

The observed angular distributions at small energy losses are bell shaped, similar to those encountered in light heavy-ion reactions near the Coulomb barrier. The angular distributions for lighter projectiles can be well described within the DWBA framework. We have performed a DWBA analysis for the one-proton stripping reactions ^{58}Ni(^{56}Fe,^{55}Mn)^{59}Cu and ^{122}Sn(^{56}Fe,^{55}Mn)^{123}Sb in order to learn to what extent these reactions can be accounted for in such a simple reaction model.

Considering the lowest excitation energy bins ($E_x \leq 9$ MeV) only, we have chosen to describe the final states of ^{59}Co and ^{123}Sb as single-proton states in the $Z=28$–50 shell and $Z=50$–82 shell, respectively. The ^{56}Fe proton was assumed to be in the $1f_{7/2}$ orbital. The calculated differential cross sections were summed over the final single-particle states for comparison to the experimental angular distributions. For simplicity all the states have been assumed to be at a binding energy of 3 MeV ($Q=-9$ MeV). The calculations were performed with the computer code ONEFF,[12] and the calculated peak cross sections for the various states are tabulated in Table IV.

Parameters for the optical model potential with an identical real and imaginary geometry were obtained from a recent study[2] of the reaction ^{86}Kr + ^{208}Pb: $V=40$ MeV; $W=25$ MeV; $r_0=1.32$ fm; and $a=0.5$ fm. The spectroscopic factor for picking up the proton in the $f_{7/2}$ shell is assumed to be 6. Bound-state wave functions for the proton were calculated in a well with $r_0=1.20$ fm and $a=0.65$ fm.

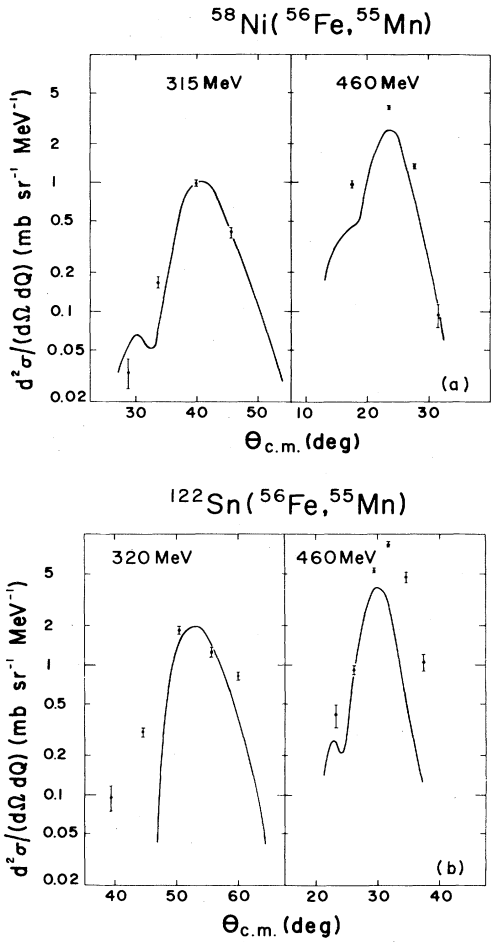

FIG. 8. (a) Angular distribution for the reaction ^{58}Ni(^{56}Fe,^{55}Mn) for $Q=-9$ MeV. The curves are results from DWBA calculations as described in detail in the text. (b) As in (a), but for the reaction ^{122}Sn(^{56}Fe,^{55}Mn).

The measured angular distributions for $Q=-9$ MeV are shown in Figs. 8(a) and (b) in comparison with calculated angular distributions. The summed calculated cross section is normalized to the data at the lower bombarding energy. The shapes of the angular distributions are well reproduced by the DWBA calculations. At more negative Q values the DWBA predictions move the peak cross section angle backwards while the experimental cross sections become more forward peaked.

At the lower bombarding energy the DWBA calculations without any external normalization account for 52% of the observed cross section in the Q-value range -4.5 to -13.5 for Fe + Ni, while for Fe + Sn they account for ~20% of the cross section (see Table IV). This agreement

is surprisingly good. It is expected that states from the next major shell contribute to the observed cross sections, and the calculations were made only for a fixed binding energy and Q value.

The dependence on bombarding energy is not described correctly. The DWBA predicts in both cases a change of roughly a factor of 2, while the experimental cross sections increase by factors of 4 and 6 for Ni and Sn, respectively.

At the low bombarding energy, close to the Coulomb barrier, the DWBA can account for the main features of the one-proton stripping reactions, i.e., the magnitude and shape of the angular distribution, while it fails at the higher energies. This may indicate that reaction mechanisms other than direct one-step processes become increasingly important as the bombarding energy becomes larger.

B. Evaporation analysis of the energy spectra

The origin of the substructures (or bumps) reported in energy spectra from symmetric heavy-ion collisions[3,4] is at present unsettled; giant resonances[3] and evaporation threshold effects[5] have been suggested. We shall examine here the latter suggestion in some detail.

The purpose of an evaporation analysis of the energy spectra is to investigate whether the substructures in the observed (secondary) energy spectra could be caused only by evaporation effects, or whether they are also present in the energy spectra prior to particle evaporation (the primary energy spectra). It is, therefore, important to use a method which minimizes the use of parametrizations of the primary spectra, since parametrization introduces constraints on the possible shapes of the spectra. We will follow a method suggested by Døssing,[13] which is similar to the methods used to unfold the effects of detector response in γ-ray spectra.

The cross section for a primary reaction product formed in some binary exit channel j with a Q value Q_n is denoted by $S^p(j,Q_n)$. The reaction angle is not noted, but in all calculations grazing angle data were used. On the way to the detector several particles (protons, neutrons, or alphas) may be emitted from the primary product. The cross section for the product actually observed in channel i corresponding to the apparent (two-body) Q value, Q_m, is $S^s(i,Q_m)$. The probability for a decay from channel j at $Q=Q_n$ to channel i at $Q=Q_m$ is $P_{ij}(Q_m,Q_n)$, and thus

$$S^s(i,Q_m)=P_{ii}(Q_m,Q_m)S^p(i,Q_m)+\sum_{j\neq i}\sum_{n=1}^{N}P_{ij}(Q_m,Q_n)S^p(j,Q_n)\ , \tag{4}$$

where the Q-value range in channel j has been divided into N equal intervals. In this expression the probabilities $P_{ii}(Q_m,Q_n)$ with $Q_m\neq Q_n$ (corresponding to gamma decay) have been neglected.

Equation (4) can be rewritten in matrix formulation by using one index (say t) to denote the final channel i and apparent Q value Q_m by setting $t=N(i-1)+m$, with m running from 1 to N and i running from 1 to some maximum channel value $j_{\max}$. A similar notation is introduced for the primary products with (t,i,m) replaced by (u,j,n). Equation (4) can then be written as

$$\underline{S}^s=\underline{P}\underline{S}^p\ , \tag{5}$$

with the definitions

$$P_{tu}=P_{ij}(Q_m,Q_n)\ ,$$
$$S^s_t=S^s(i,Q_m)\ ,$$
$$S^p_u=S^p(j,Q_n)\ ,$$

where $t=N(i-1)+m$ and $u=N(j-1)+n$. The matrix $\underline{P}$ is a quadratic upper triangular matrix (if the sequence of channel numbers is suitably chosen) of rank $Nj_{\max}$. Due to the large order of $\underline{P}$ (typically 250—350) the set of equations (5) have to be solved by an iterative method that minimizes the Euclidean norm of the residual

$$||R||=||\underline{P}\underline{S}^p-\underline{S}^s||$$

with respect to $\underline{S}^p$. We have used the over-relaxed Gauss-Seidel method,[14] which gives rapid convergence but is limited to situations in which the diagonal elements of $\underline{P}$ are not too small. Since the diagonal elements express the probability for no particle decay, this limits the calculations in most cases to Q values larger than -40 MeV. Since the substructures are fully covered by this Q-value interval, this restriction is not a problem in the present calculations. If $\underline{P}$ can be constructed, we can deduce the primary spectra from the observed secondary spectra and thus determine if an observed substructure may have originated from a structure in the primary spectrum or may have been created from a smooth primary spectrum.

The construction of $\underline{P}$, however, is not unique insofar as we do not know the distribution of excitation energy among the primary reaction products. We have used a Gaussian distribution for the probability that the primary projectilelike reaction fragment A receives an excitation energy E_A.[15] Thus,

$$P(E_A)\simeq\exp[-0.5(E_A-\bar{E}_A)^2/\sigma^2_{(E_T)}]\ , \tag{6}$$

where E_T is the total excitation energy of both fragments A and B and E_A is constrained by $0\leq E_A\leq E_T$. The average excitation energy in A is

$$\bar{E}_A=\delta[a_A/(a_A+a_B)]E_T\ ; \tag{7}$$

a_A and a_B are the usual Fermi-gas level density parameters and were chosen to be $A/8$ MeV^{-1}. Finally, the width of the excitation energy distribution in A was taken as

$$\sigma^2_{(E_T)}=2\beta^2(E_T)^{3/2}\frac{a_Aa_B}{(a_A+a_B)^{5/2}}\ . \tag{8}$$

Equations (6)—(8) with $\delta=\beta=1$ are valid for the limiting case in which the two nuclei are in thermal equilibrium and the level density in each nucleus is of the form

$$\rho(E^*)=\exp(2[aE]^{1/2})\ , \tag{9}$$

independent of the angular momentum. The parameter δ can vary from 0 (all excitation energy in nucleus B) to $(a_A+a_B)/a_A$ (all excitation energy in A). β can be used to

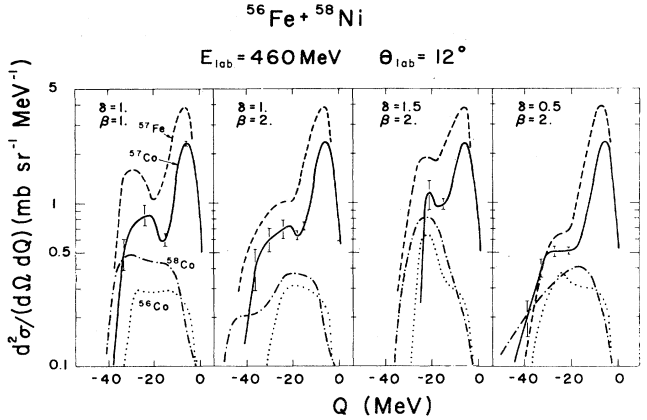

FIG. 9. Calculated primary spectra for ^{57}Fe and ^{56,57,58}Co in the reaction ^{56}Fe + ^{58}Ni at 460 MeV. The parameters δ and β are explained in the text. The error bars indicate the uncertainties introduced in the primary ^{57}Co spectra by the statistical uncertainties in the measured secondary spectra.

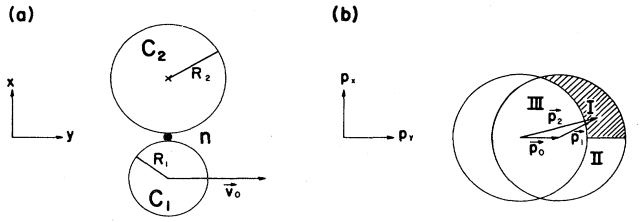

FIG. 10. (a) Schematic picture of the geometrical configuration of the transfer process at the distance of closest approach. (b) Schematic picture of the two overlapping Fermi spheres in the momentum space. For simplicity, only the x-y plane is shown. p_0 is the displacement of the two momentum distributions due to the relative translational motion; p_1 and p_2 are the momenta of the transferred nucleon relative to the cores c_1 and c_2, respectively. Only if the nucleon's momenta are situated in region I is a transfer from c_1 to c_2 possible. Momenta in region II have the wrong direction, and momenta in region III are blocked due to the Pauli principle.

vary the width of the excitation energy distribution.

With these prescriptions, the P matrix was calculated with the Monte Carlo evaporation code LILITA (Ref. 16) for a large number of values for δ and β in the intervals $0 \le \delta \le 2$ and $0 \le \beta \le 10$. The calculations include recoil effects of the emitted particles on the fragment kinetic energy and direction. The shift and the broadening of the angular distributions with increasing energy loss has also been included by parametrizing the observed experimental angular distributions. Q-value bins of 3 MeV were used, and 13 reaction channels were included (^{57,58,59,60}Ni, ^{55,56,57,58,59,60}Co, ^{57,58,59}Fe). The truncation of the reaction channels resulting from exclusion of ^{54,55,56}Fe was necessary, since the corresponding spectra were contaminated by slit scattering. As a consequence of this restriction the $Z = 24$ or 25 reaction products could not be included either.

The deduced primary spectra for ^{57}Fe and ^{56,57,58}Co are shown in Fig. 9 for a few values of δ and β. For all investigated choices of δ and β, the $Q \approx -25$ MeV substructures of the secondary spectra are found to originate from structures in the deduced primary spectra of ^{57}Fe and ^{57}Co. For the other nuclei the spectral shapes are much more strongly dependent on β and δ, and no unique conclusion can be drawn.

Under the assumption that the parametrization in Eqs. (6)—(8) is realistic, the conclusion of our evaporation analysis is that evaporation effects alone cannot quantitatively explain the substructures observed in the one-nucleon pickup channels, and other mechanisms more directly related to the primary collision process have to be incorporated.

C. Optimum Q values

The observed Q_{opt} values may be examined within a simple model based on the classical Brink picture.[17] The model includes Pauli blocking, which has been demonstrated by Randrup[18] and the Rochester group[19] to be essential in considering energy losses induced by nucleon transfer. As a novel feature, the magnitude of the Pauli blocking effects are calculated by use of the local Fermi momentum in the surface region of the nucleus.

Consider the transfer of a nucleon n with mass m from a core c_1 of mass m_1 to another core c_2 of mass m_2. It is assumed that the transfer is localized to a point directly between the two nuclei, as shown in Fig. 10(a), and takes place at the distance of closest approach. This situation corresponds to the classical Brink picture. The relative velocity $\vec{v}_0$ of (c_1+n) and c_2 just before the transfer will then be tangential, and the kinetic energy is

$$e_i = 0.5\mu_i v_0^2 = E_{\text{c.m.}} - V_B^i(R) , \tag{10}$$

where μ_i is the reduced mass in the entrance channel, $E_{\text{c.m.}}$ is the center-of-mass energy at infinity, and $V_B^i(R)$ is the interaction potential at the distance R, as determined from Eqs. (2)—(3). In the following a coordinate system is introduced with the y axis in the direction of $\vec{v}_0$ and the x axis directed from the center of c_1 to the center of c_2 at the moment of transfer [see Fig. 10(a)]. The translational momentum of n relative to c_2 is

$$\vec{p}_0 = m\vec{v}_0 .$$

In addition to $\vec{p}_0$, n will, at the time of transfer, have an internal momentum $\vec{p}_1$ in its motion relative to c_1, so the transferred momentum from c_1 to c_2 will be

$$\vec{p}_2 = \vec{p}_0 + \vec{p}_1 .$$

If we define $\Delta e = e_f - e_i$, where e_f is the kinetic energy at the barrier in the final channel, it follows from momentum conservation that

$$\Delta e = -m\frac{e_i}{\mu_i}[1 - m/(m+m_2)](1 + 2p_{1y}/p_0) + e_i\frac{m^2}{\mu_i\mu_f}p_1^2/p_0^2 . \tag{11}$$

p_{1y} is $\vec{p}_1$'s component along the y direction. For heavy-ion collisions with bombarding energies above the barrier, the first term dominates. Equation (11) expresses the kinetic energy loss at the barrier for a transfer with a well-defined value of $\vec{p}_1$. We further assume that the average kinetic energy loss on the barrier equals the $Q_{\rm opt}^{\rm eff}$ value. In order to calculate $Q_{\rm opt}^{\rm eff}$, it is therefore necessary to average over all possible values of $\vec{p}_1$ contributing to the transfer process.

$$Q_{\rm opt}^{\rm eff}=-\alpha m e_i/\mu_i \ ,$$

where

$$\alpha=[1-m/(m+m_2)](1+2\langle p_{1y}\rangle/p_0) - \frac{m}{\mu_f}(\langle p_1^2\rangle/p_0^2) \ . \tag{12}$$

As was pointed out by Randrup,[18] it is essential to include Pauli blocking effects. In Fig. 10(b) the Fermi spheres of c_1 and c_2 are shown schematically. Only $\vec{p}_1$ momenta in the shaded volume (I) will contribute to the transfer process. Momenta in volume II will have a direction away from the acceptor nuclei, and momenta in volume III cannot be accepted in c_2 due to the Pauli principle. The Fermi spheres will, in general, have a diffuse boundary determined by the temperature τ of the system. Additional contributions to the diffusivity of the Fermi spheres originating from pairing interactions and from the diffuseness of the nuclear potential will be ignored.

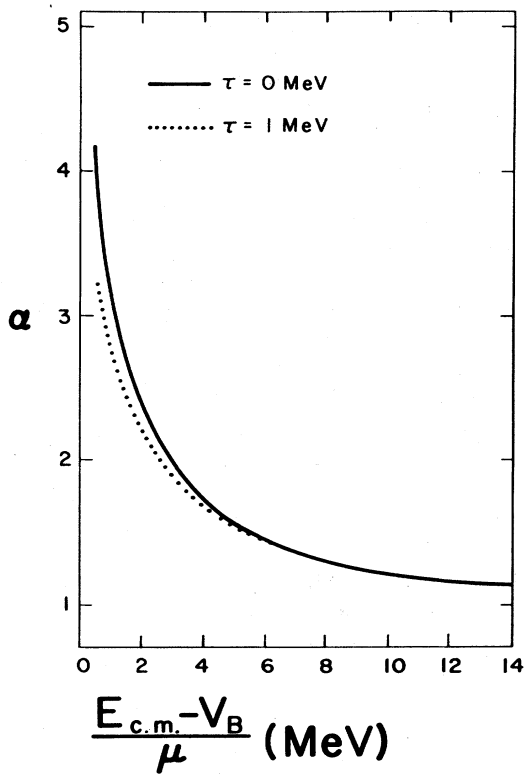

FIG. 11. The factor α as a function of the available energy on the barrier per nucleon. The curves are calculated under the assumption that the local Fermi momentum is 0.6 fm^{-1}.

Due to the assumed localization of the transfer process in R space, the radius of the Fermi spheres P^F is the local Fermi momentum in the surface regions of the colliding nuclei. P^F can be estimated in the Thomas-Fermi (TF) approximation, where it is determined by the local nucleon density $\rho(r)$ via the relation

$$P_{\rm TF}^F(r)=[\tfrac{3}{2}\pi^2\rho(r)]^{1/3} \ . \tag{13}$$

$\rho(r)$ is parametrized by a Woods-Saxon form factor with parameters[20] $\rho_0=0.17$ fm^{-3}, $R_\rho=1.1A^{1/3}$ fm, and $a_\rho=0.54$ fm. At the grazing angle the transfer is localized to the vicinity of [see Eq. (3)]

$$R=1.07A^{1/3}+1.36 \text{ fm} \ .$$

For the nuclei of interest the local Fermi momentum at the radius R is

$$p^F(R)\sim 0.6 \text{ fm}^{-1} \ . \tag{14}$$

It is now assumed that the probability P for a given momentum $\vec{p}_1$ to contribute in the transfer process is given by

$$\begin{aligned} P(\vec{p}_1)&=Cf_1(p_1)\bar{f}_2(p_2)f_{\rm flux} \ , \\ f_1(p_1)&=\left[1+\exp\left[\frac{p_1^2-(p^F)^2}{2m\tau}\right]\right]^{-1} \ , \\ \bar{f}_2(p_2)&=\left[1+\exp\left[-\frac{p_2^2-(p^F)^2}{2m\tau}\right]\right]^{-1} \ , \\ f_{\rm flux}&=\begin{cases} p_{1x} & \text{if } p_{1x}>0 \\ 0 & \text{if } p\le 0 \ . \end{cases} \end{aligned} \tag{15}$$

f_1 is the occupation probability in c_1, and $\bar{f}_2$ is the vacancy probability in c_2. The flux factor $f_{\rm flux}$ accounts for the fact that, for a fixed interval of time, the transfer probability depends on the magnitude of the velocity in the direction from the donor to the acceptor. C is a normalization constant. By calculating the average of p_{1y} and p_1^2 over the Fermi sphere of c_1 with the probability function $P(\vec{p}_1)$, the factor α can be obtained from Eq. (12). If Pauli blocking is not taken into account, $\alpha\approx[1-m/(m+m_2)]$.

Figure 11 shows α (with Pauli blocking) as a function of e_i/μ_i for $\tau=0$ and 1 MeV. It is seen that the energy loss per transferred nucleon is strongly enhanced due to Pauli blocking for the small relative velocities, but as the temperature increases, the effect becomes gradually smaller.

In order to calculate $Q_{\rm opt}^{\rm eff}$ for the transfer of several nucleons, it is assumed that the nucleons are transferred sequentially. After the jth transfer, the relative kinetic energy is

$$\begin{aligned} e_{j+1}&=e_j-m\frac{e_j}{\mu_j}\alpha_j \\ &=e_j\left[1-m\frac{\alpha_j}{\mu_j}\right] \ , \end{aligned}$$

and the temperature τ is

$$\tau \simeq \left[\frac{8(e_1 - e_j)}{m_1 + m_2 + m} \right]^{1/2},$$

where e_1 is the initial nucleon kinetic energy.

The $Q_{\text{opt}}^{\text{eff}}$ for the transfer of N nucleons sequentially can then be written

$$Q_{\text{opt}}^{\text{eff}} = -e_1 \left[1 - \prod_{j=1}^{N} \left[1 - m\frac{\alpha_j}{\mu_j} \right] \right]. \quad (16)$$

If α_j/μ_j is approximately constant, then

$$Q_{\text{opt}}^{\text{eff}} \sim -e_1 \left[1 - \left[1 - m\frac{\alpha}{\mu} \right]^N \right] \quad (17)$$

so $Q_{\text{opt}}^{\text{eff}} \to -e_1$ for $N \to \infty$.

In Fig. 12 the experimental $Q_{\text{opt}}^{\text{eff}}$ values are plotted versus the number of transferred nucleons ΔM. For a given value of ΔM, there are often quite large differences in the $Q_{\text{opt}}^{\text{eff}}$ values. These variations, which are strongly correlated to differences in ground-state–ground-state Q values, cannot be described within the present model, because it does not include any explicit dependence on the nuclear structure of the colliding nuclei.

In Fig. 12 are also shown three sets of model predictions. If Pauli blocking effects are completely ignored (dotted curves) the calculated energy losses are too small, especially at the low bombarding energies. On the other hand, if α is calculated with the global nuclear Fermi momentum 1.36 fm^{-1} (dotted-dashed curves), then the estimated energy losses are too large. The results, using the local Fermi momentum $P_1^F = 0.6$ fm^{-1} [Eq. (14)], are shown as dashed curves and give a good description of the magnitudes of the $Q_{\text{opt}}^{\text{eff}}$ values as a function of the number of transferred nucleons, the bombarding energy, and the target nucleus.

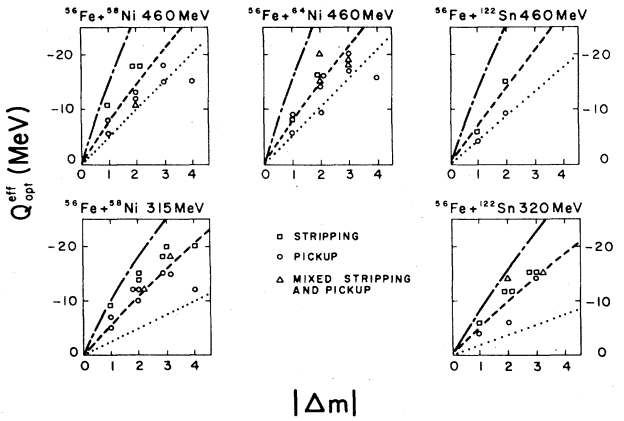

FIG. 12. Experimental $Q_{\text{opt}}^{\text{eff}}$ as function of the number of transferred nucleons ΔM. The lines refer to different model predictions: no Pauli blocking (dotted); Pauli blocking calculated with $p^F = 1.36$ fm^{-1} (dotted-dashed); and Pauli blocking calculated with $p^F = 0.6$ fm^{-1} (dashed).

V. SUMMARY AND CONCLUSIONS

Differential cross sections $\sigma(Z,A,E,\theta)$ have been measured for the projectilelike fragment resulting from ^{56}Fe bombardment of ^{58,64}Ni and ^{122}Sn at energies of 5.9 and 8.5 MeV/nucleon.

The angular distributions, which are bell shaped in the quasielastic region, could for the one-proton stripping reaction at $Q = -9$ MeV be well reproduced with a DWBA calculation. At the lower bombarding energy the DWBA calculations could account for $\sim 50\%$ of the experimental cross section in the ^{56}Fe + ^{58}Ni case while the corresponding number for ^{56}Fe + ^{122}Sn was 20%. The experimental cross section showed a stronger bombarding energy dependence than predicted from the DWBA calculations.

Besides the quasielastic and deep-inelastic components, some energy spectra exhibit a substructure for Q values around -25 MeV. At larger energy losses no substructures were found. The substructures are most prominent at the high bombarding energy and in the one-nucleon pickup channel.

The effects of evaporation on the observed spectra were unfolded with the use of statistical model calculations and a simple parametrization of the energy sharing between the two fragments. It was concluded that, given the present assumptions of the model, the observed substructures are present in the energy spectra prior to evaporation and arise from the primary collision process.

The $Q_{\text{opt}}^{\text{eff}}$ values varied roughly linearly with the number of transferred nucleons, indicating a fixed energy loss per transferred nucleon for a given reaction. The general trends of the measured $Q_{\text{opt}}^{\text{eff}}$ values can be understood within the simple classical Brink picture combined with the idea of Pauli blocking. Reasonable agreement with the experimental data was obtained when the magnitude of the Pauli blocking effects was determined, not by the global Fermi momentum of the nucleus, but by the local Fermi momentum in the region of the nuclear surface where the transfer process is localized.

ACKNOWLEDGMENTS

It is a pleasure to acknowledge helpful discussions with T. Døssing and J. Randrup. We are indebted to M. Blann for his help during the experiments and to J. Gomez del Campo for providing us with a version of his Monte Carlo evaporation code LILITA. We gratefully acknowledge the help of the SuperHILAC staff and user-support organization. S.P. acknowledges the support of the Danish Natural Science Research Council. This work was supported in part by the Danish Natural Science Research Council and in part by the U.S. Department of Energy.

*Present address: Physics Department, Brookhaven National Laboratory, Upton, New York 11973.

†Present address: PNN, CEA, Bruyeres le Chatel, 92542 Montrouge, France.

[1] U. Arlt, R. Bass, V. Hartmann, R. Renfordt, K. Sapotta, P. Fröbrich, and W. Schäfer, Phys. Rev. C 22, 1790 (1980).

[2]Jiang Cheng-Lie, P. R. Christensen, Ole Hansen, S. Pontoppidan, F. Videbaek, D. Schull, Shen Wen-Qing, A. J. Baltz, P. D. Bond, H. Freiesleben, F. Busch, and E. R. Flynn, Phys. Rev. Lett. 47, 1039 (1981).

[3]N. Frascaria, C. Stephan, P. Colombani, J. P. Garron, J. C. Jacmart, M. Riou, and L. Tassan-Got, Phys. Rev. Lett. 39, 918 (1977); H. Tricoire, P. Colombani, G. Gerschel, D. Paya, N. Perrin, L. Valentin, N. Frascaria, J. P. Garron, and C. Stephan, J. Phys. Lett. 40, 181 (1979); N. Frascaria, P. Colombani, A. Gamp, J. P. Garron, M. Riou, J. C. Roynette, C. Stephan, A. Ameaue, C. Bizard, J. L. Laville, and M. Louvel, Z. Phys. A 294, 167 (1980).

[4]A. C. Mignerey, H. Breuer, V. E. Viola, K. L. Wolf, B. G. Glagola, W. W. Wilcke, W. U. Schroeder, J. R. Huizenga, and J. R. Birkelund, Bull. Am. Phys. Soc. 25, 482 (1980); A. C. Mignerey, K. L. Wolf, H. Breuer, B. G. Glagola, V. E. Viola, J. R. Birkelund, D. Hilscher, J. R. Huizenga, W. U. Schroeder, and W. W. Wilcke, *Proceedings of the International Conference on Nuclear Physics, Berkeley, California, 1980,* edited by R. M. Diamond and J. O. Rasmussen (North-Holland, Amsterdam, 1981).

[5]D. Hilscher, J. R. Birkelund, A. D. Hoover, W. U. Schroeder, W. W. Wilcke, J. R. Huizenga, A. C. Mignerey, K. L. Wolf, H. F. Breuer, and V. E. Viola, Phys. Rev. C 20, 556 (1979).

[6]H. C. Britt, B. H. Erkkila, A. Gavron, Y. Patin, R. H. Stokes, M. P. Webb, P. R. Christensen, Ole Hansen, S. Pontoppidan, F. Videbaek, R. L. Ferguson, F. Plasil, G. R. Young, and J. Randrup, Phys. Rev. C 26, 1999 (1982).

[7]F. Plasil, R. L. Ferguson, H. C. Britt, B. H. Erkkila, P. D. Goldstone, R. H. Stokes, and H. H. Gutbrod, Phys. Rev. C 18, 2603 (1978); G. Gabor, W. Schimmerling, D. Greiner, F. Bieser, and P. Lindstrom, Nucl. Instrum. Methods 130, 65 (1975).

[8]P. R. Christensen, F. Folkmann, Ole Hansen, O. Nathan, N. Trautner, F. Videbaek, S. Y. van der Werf, H. C. Britt, R. P. Chestnut, H. Freiesleben, and F. Pühlhofer, Nucl. Phys. A349, 217 (1980).

[9]P. Glassel, R. C. Jared, and L. G. Moretto, Nucl. Instrum. Methods 142, 569 (1977).

[10]*Heavy Ion Collisions,* edited by R. Bock (North-Holland, Amsterdam, 1980).

[11]P. R. Christensen and A. Winther, Phys. Lett. 65B, 19 (1976); R. A. Broglia and A. Winther, *Heavy Ion Reactions,* (Benjamin, New York, 1981), Vol. I.

[12]R. A. Broglia, R. Liotta, B. S. Nilsson, and A. Winther, Phys. Rep. 29, 291 (1977).

[13]Th. Døssing (private communication).

[14]N. Gastinel, *Linear Numerical Analysis* (Academic, New York, 1970).

[15]D. J. Morrissey and L. G. Moretto, Phys. Rev. C 23, 1835 (1981).

[16]J. Gomez del Campo, R. G. Stokstad, J. A. Biggerstaff, R. A. Dayras, A. H. Snell, and P. H. Stelson, Phys. Rev. C 19, 2170 (1979); J. Gomez del Campo, Oak Ridge report, 1979 (unpublished).

[17]D. M. Brink, Phys. Lett. 40B, 37 (1972).

[18]J. Randrup, Nucl. Phys. A307, 319 (1978); A327, 498 (1979).

[19]W. U. Schröder, J. R. Birkelund, J. R. Huizenga, W. W. Wilcke, and J. Randrup, Phys. Rev. Lett. 44, 308 (1980); W. W. Wilcke, J. R. Birkelund, A. D. Hoover, J. R. Huizenga, W. U. Schröder, V. E. Viola, K. L. Wolf, and A. C. Mignerey, Phys. Rev. C 22, 128 (1980).

[20]A. Bohr and B. Mottelson, *Nuclear Structure* (Benjamin, New York, 1969), Vol. 1.